Acetazolamide loaded-silver nanoparticles: A potential treatment for murine trichinellosis

E.F. Abdel Hamed ⬡, A.A. Taha, S.M. Abdel Ghany, A.A. Saleh and E.M. Fawzy

Department of Medical Parasitology, Faculty of Medicine, Zagazig University, Sharkia, Egypt

Abstract

Trichinellosis is a global food-borne disease caused by viviparous parasitic nematodes of the genus *Trichinella*. Due to the lack of effective, safe therapy and the documented adverse effects of traditional therapy, this study aimed to evaluate the therapeutic effect of acetazolamide-loaded silver nanoparticles (AgNPs) on murine trichinellosis. Fifty male Swiss albino mice were divided into five groups of ten mice each: Group I, normal control group; Group II, infected with *T. spiralis* and not treated; Group III, infected and given AgNPs; Group IV, infected and treated with acetazolamide; and Group V, infected and treated with acetazolamide-loaded AgNPs. Mice were infected orally with 250 larvae. The efficacy was assessed by counting *T. spiralis* adults and larvae, measuring serum total antioxidant capacity, and observing the histopathological and ultrastructural alterations. Acetazolamide-loaded AgNPs treatment exhibited the highest percentage of reduction (84.72% and 80.74%) for the intestinal adults and the muscular larvae of *T. spiralis*-infected animals, respectively. Furthermore, during the intestinal and muscular phases, the serum of the same group had the best free-radical scavenging capacity (antioxidant capacity), which reduced tissue damage induced by oxidative stress. Histopathologically, the normal intestinal and muscular architecture was restored in the group treated with acetazolamide-loaded AgNPs, in addition to the reduced inflammatory infiltrate that alleviated inflammation compared to infected animals. Our results confirmed the marked destruction of the ultrastructural features of *T. spiralis* adults and larvae. Acetazolamide-loaded AgNPs are a promising therapy against *T. spiralis* infection.

Introduction

A common and serious food-borne parasite disease called trichinellosis is brought on by eating raw, undercooked animal meat that contains infected *Trichinella* nematode larvae (Bai *et al.* 2017; Luis Muñoz-Carrillo *et al.* 2019). *Trichinella* causes a wide range of illnesses, infecting over 150 animals as well as humans (Pozio *et al.* 2015). Human trichinellosis can be acute or chronic. The clinical symptoms of an acute stage include headache, fever, and gastrointestinal problems. The chronic stage may involve myositis caused by larval growth in skeletal muscles and can be severe, painful, or incapacitating. Furthermore, muscle dysfunction and discomfort might have a long-term impact on patients (Dupouy-Camet 2014). Furthermore, encephalitis and secondary infections, such as bronchopneumonia or sepsis, can occur. Symptom duration depends on the infection dose and the severity of the illness (Gottstein *et al.* 2009). Trichinellosis harms human health, raises concerns about food safety, and can result in significant financial losses. Consequently, finding a cure is vital. Trichinellosis infection is traditionally treated with albendazole (Gottstein *et al.* 2009). Although it is fatal to *Trichinella* adults, its limited bioavailability reduces the likelihood of killing encapsulated larvae (Eid *et al.* 2020). Still, it can cause serious systemic reactions – for instance, encephalitis, seizures, drug allergies, and even fatalities (Yada v*et al.* 2012).

Acetazolamide is a sulfonamide that inhibits carbonic anhydrase. Most insect and nematode species, including *Ancylostoma caninum*, *Ascaris spp.*, *Entamoeba spp.*, *Necator americanus*, and *T. spiralis*, include beta-carbonic anhydrases (β-CAs), which are most likely mitochondrial enzymes (Zolfaghari-Emameh *et al.* 2014). Inhibition of nematode β-CAs offers chances to treat or control many parasitic infections with negligible adverse effects on the hosts (Zolfaghari-Emameh *et al.* 2015). Acetazolamide, one of the CAs inhibitors used against *T. spiralis*, can interact with metabolic processes and potentially eliminate pathogens (Syrjänen *et al.* 2010).

By combating poor cellular permeability, nonspecific distribution, low bioavailability, and the quick clearance of drugs against parasites out of the body, silver nanoparticles, a new emerging drug carrier, are helpful in treating a number of parasitic disorders. AgNPs displayed antiparasitic efficacy against a wide range of parasites, including *Fasciola* (Gherbawy *et al.* 2013), filaria (Saini *et al.* 2016), *Leshmania* (Allahverdiyev *et al.* 2011), *Cryptosporidium parvum*, *Entamoeba histolytica* (Saad *et al.* 2015), *Blastocystishominis* (Younis *et al.* 2020), *Plasmodium*, *Toxoplasma*, *Giardia*, and insect larvae (Elmi *et al.* 2013), and were also used as antimicrobial therapies (Sun *et al.* 2019).

The total antioxidant capacity (TAOC) is a quantitative assay that indicates the cumulative impact of primarily non-enzymatic antioxidants found in plasma and body fluids (Ghiselli et al. 2000). The TAOC measurement could offer details about the balance of oxidants and antioxidant systems (Collins 2005). An insufficient antioxidant capability may contribute to excessive tissue damage. Improved antioxidant capacity may assist the host by reducing tissue damage caused by oxidative stress, reducing the severity of symptoms and the development of complications, and allowing the body to maintain a functioning immune system capable of eradicating the infection (Akaike et al. 1998).

The goal of this study was to evaluate acetazolamide-loaded silver nanoparticles in the treatment of *T. spiralis* infection in mice by investigating the parasite load as well as histopathological and ultrastructural alterations in the gut and muscle phases of the parasite, in addition to measuring serum TAOC.

Materials and methods

Parasites and doses of infections

The *Trichinella spiralis* strain (Istituto Superiore di Sanità code: ISS6158) was obtained from the Parasitology Department, Faculty of Medicine, Zagazig University. The infective dose of 250 of larvae was given to each mouse (Chen *et al.* 2012). Mice were starved for 12 hours before being infected and then fed the larvae.

Experimental design

Five groups of male Swiss albino mice of matched age (6 weeks) and weight (20–25 g) were used. Each group consisted of ten mice: Group I, control normal; Group II, infected with *T. spiralis* and not treated; Group III, infected, then treated with nanoparticles; Group IV, infected at that time and treated with acetazolamide; Group V, infected and subsequently treated with acetazolamide-loaded nanoparticles. Every group was subdivided into two subgroups of five mice each: group a, for detection of the intestinal phase (adults), mice were sacrificed six days post-infection (P.I.), and group b, for detection of the muscular phase (larvae), mice were sacrificed 45 days P.I. (AbouRayia *et al.* 2017).

Drugs

Acetazolamide in the form of 250-mg tablets (Cidamex, Chemical Industries Development (CID), Egypt, Giza) was dissolved in distilled water, and 100 mg/kg/day was orally given (Saad *et al.* 2016). About 50 mg/kg/day of acetazolamide-loaded nanoparticles were administered orally. Nearly 200 µg/mice of nanoparticles were orally given. Subgroup (a) received drugs on the second post-infection day for four consecutive days, whereas subgroup (b) received treatments on the 12th post-infection day for four days.

Nanoparticles preparation

An Erlenmeyer flask was filled with 30 L of 0.002M (NaBH4). For around 20 minutes, the flask was placed on a stir plate with a magnetic stir bar in an ice bath. A total of 2 mL of 0.001 M (AgNO3) was dripped into the swirling NaBH4 solution at a rate of about 1 drop per second, stopping after all of the AgNO3 was

introduced. A few drops of 1.5 M NaCl solution were added to the suspension, causing it to darken yellow and eventually grey as the nanoparticles accumulated. In order to prevent aggregation, 0.3% PVP was added. To leave air bubbles and undissolved PVP in the beaker, the liquid was decanted into a mold. The liquid was then placed in a toaster oven for 30 minutes to evaporate (Mulfinger *et al.* 2007).

Characterization of silver nanoparticles

AgNP was characterized by its size and shape (Fisker *et al.* 2000).

- Morphology and particle size determination

Scanning electron microscopy (SEM) analysis was performed after AgNP preparation by the LEO 1430 VP SEM machine. To prepare thin films of the sample on a carbon-coated copper grid, a small amount of the sample was added. Blotting paper was used to get rid of the extra solution. Afterward, the film was dried under a mercury lamp on the SEM grid (Ziel *et al.* 2008).

- Fourier-transform infrared spectroscopy analysis

The synthesized Ag nanoparticle solution was centrifuged at 3000 rpm for 30 min to prepare AgNPs in powder form. The AgNPs-containing pellet was dispersed three times using sterile deionized water to remove biological contaminants and free proteins and enzymes, not capping ligands for AgNPs. The samples were dried overnight in an oven at 60°C, ground with KBr pellets, and evaluated on a Bruker Tensor 27 model at a resolution of 4 cm in the diffuse reflectance mode (Mulvaney 1996).

Preparation of acetazolamide-loaded nanoparticles

Acetazolamide-loaded nanoparticles were produced by adding silver nanoparticles to a solution containing 50 mg/ml acetazolamide concentrations. After centrifugation of the sample at 20,000 g at 14°C for 30 minutes, it was separated from the aqueous suspension. The Bradford protein assay spectrophotometric method was used to detect the protein concentration (free) in the supernatant at 595 nm. The loading capacity (LC) and encapsulation efficiency (EE) of nanoparticles were analysed as follows (Mulfinger *et al.* (2007):

$$\%EE = [(A\text{-}B)/A] \times 100$$
$$\%LC = [(A\text{-}B)/C] \times 100'$$

where A is the total amount of drugs, B is the free amount of drugs, and C is the weight of nanoparticles.

Mortality rate (MR%)

At the 6th and 54th days post-infection, the mortality rate was estimated according to the present equation: MR% = number of dead mice at the sacrifice time/number of mice at the beginning of the experiment X100 (Eissa *et al.* 2012).

T. spiralis adults count in the intestine

The cleaned intestine was cut into 1-cm sections and incubated in 10 mL of saline for 2 hours at 37°C to allow the worms to move out of the tissue and gather in the container. The intestine was rinsed a number of times with pipetted saline. The fluid was gathered and

centrifuged at 1500 rpm for 5 minutes. For counting the worms, the sediment was dissolved in drops of saline before being inspected drop by drop under a 10x microscope. (Issa *et al.* 1998).

Counting T. spiralis larvae

About 200 ml of distilled water with 1% pepsin hydrochloride was used to digest the dissected mice. The encysted larvae were collected using the sedimentation method after one hour of incubation at 37° C with continuous stirring with an electric stirrer (**Denham 1965**). A McMaster counting chamber was used for counting larvae in three samples of 0.1 mL (10x objective). To calculate the number of larvae per gram of tissue, the average of three counts was used (Abou Rayia *et al.* 2017). The efficacy of drugs was evaluated by comparing the number of larvae per gram retrieved from infected groups.

Assessment of serum TAOC

During the sacrification process, the collection of neck vein blood was done using the capillary tube on the 6th day of P.I. for subgroup a (intestinal phase) and on the 45th day of P.I. for subgroup b (muscular phase). The samples were left for 10 to 20 minutes to clot at room temperature. To get serum samples, these clots were removed using centrifugation for 20 minutes at 2000–3000 rounds per minute. TAOC was measured by an ELISA kit (Biospes Company, Jiulongpo Industry District, Chongqing, China) according to the manufacturer's instructions (Wang *et al.* 2017).

Histopathological study

Fixation in formalin 10%, paraffin sectioning, and hematoxylin and eosin (H&E) staining were processed for the intestinal, lingual, and skeletal muscles of mice (Carleton *et al.* 1967). The presence of inflammatory reactions, nurse cells, and encapsulated *T. spiralis* larvae was blindly observed under a microscope (IX73, Olympus, Japan).

Scanning electron microscopy

The adults and larvae were incubated at 4°C overnight in a fixed solution (2.5% glutaraldehyde). Adults were washed for 5 minutes in 0.1 M sodium cacodylate buffer and fixed in 2% osmium tetroxide for 1 hour. The samples were dehydrated in ascending grades of alcohol and dried using a critical point of carbon dioxide drying. After sputter coating with gold, a scanning electron microscope (Hitachi SU8040, Japan) was used to observe the samples.

Statistical analysis

The data were analyzed by the SPSS (Statistical Package for the Social Sciences) version 26. The differences between the treated and control groups were analyzed using a one-way analysis of variance (ANOVA). Data are expressed as the mean ± standard deviation (SD) of at least three repeated experiments. Values with a p<0.05 were considered statistically significant. In all cases, p-values were expressed as [#]p<0.05, [##]p< 0.01, and [###]p<0.001.

Results

AgNPs morphology and particle size

SEM revealed that the conjugation of nanoparticles with the drug (Figure 1a) had no impact on the morphology of nanoparticles alone. Most nanoparticles were spherical in shape with a smooth surface. The size distribution of nanoparticles was 40 nm for about 50%, 60 nm for 20%, and 60–90 nm for the remaining percentages. The concentration of nanoparticles was 2.33×10^8 particles/ml as estimated by UV/visible spectrophotometry using Beer's law. The surface plasmon resonance (SPR) peak can be seen as a symmetrical peak with a maximum of 520 nm.

The mortality rate

During the intestinal phase, the mortality rates revealed that mice in GI and GV survived the whole experiment, while 10% of mice in GII, GIII, and GIV died. In the muscular phase, no mortality was detected in GI and GV, but the mortality rate was 20% in GII, and GIII, while it was 10% in GIV (Table 1).

The number of adult worms in the small intestine and larvae in the muscles

The lowest mean adult worms and larvae count were attained in GV, with the highest percentage reduction of 84.72% and 80.74%, respectively, with a statistically significant difference (P<0.001) compared to the control-infected group, followed by GIV, with a percentage reduction of 61.32% and 60.47%, respectively. GIII exhibited the highest mean adult worm and larvae count with a percentage reduction of 15.95% and 14.87%, respectively, with a statistically significant difference (P<0.01) compared to the control-infected group (Table 1).

Serum TAOC assay

The highest mean blood TAOC levels in the intestinal and muscular stages were in GV, followed by GIV. There was also a statistically significant difference (P<0.001) in these groups compared to the control infected and the control healthy groups. There was a slight increase in the serum TAOC levels of GIII with a high statistically significant difference (P<0.001) compared to the control infected group (Table 2).

Results of the histopathological study

Small intestine findings

The small intestine of GVa exhibited mild mucosal invasion by degenerated *Trichinella* adult, normal intestinal villi, and mild mucosal and submucosal infiltrations by lymphocytes along with intact mucosa (Figure 2h, i), compared to the intense invasion by *T. spiralis* adult in GII, triggering pressure atrophy in the cells, and mucosal edema with an excessive inflammatory reaction – mostly lymphocytes in the surrounding intestinal mucosa (Figure 2b, c). Subsequently, GIVa revealed moderate mucosal invasion by degenerated *Trichinella* adults with moderate mucosal and submucosal infiltration by lymphocytes and eosinophils. Goblet cells appear hyperreactive (Figure 2e, g). However, GIIIa showed edematous intestinal villi, pressure atrophy of the mucosal epithelium, and severe mucosal infiltration by lymphocytes and eosinophils (Figure 2d, e).
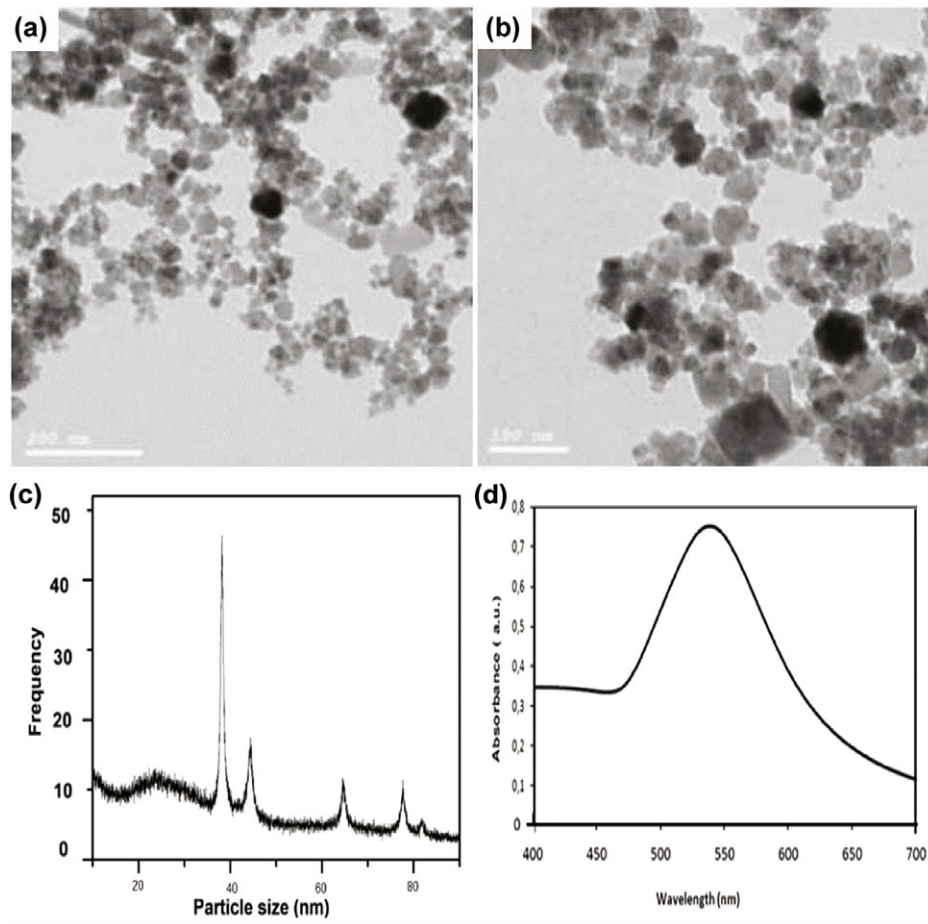
Figure 1. The morphology and particle size determination of silver nanoparticles. a, b: SEM showed that the conjugation of nanoparticles with drugs did not affect the morphology of nanoparticles alone. c: FTIR spectra of nanoparticles show that 50% of nanoparticles were approximately about 40 nm and 20% were approximately about 60 nm, while the remaining percent ranged from 60 to 90 nm. d: UV/visible spectrophotometry determined the concentration of nanoparticles was to be 2.33X108 particles/ml by using Beer's law. The surface plasmon resonance (SPR) peak can be seen as a symmetrical peak with a maximum at 520 nm.

Table 1. Adult and larval counts and the mortality during the intestinal and muscular phases of *T. spiralis*-infected groups

Groups	Intestinal phase Mean ± SD range R%	F	P	Mortality rate	Muscular phase Mean ± SD	F	P	Mortality rate
GI				0%				0%
GII	87.2 ± 6.5 79–95	436.204	<0.001 (HS)	10%	98.6 ±3.0 96–102	882.584	<0.001 (HS)	20%
GIII	73.3±3.0[##] 70–76 15.95%			10%	84.0 ±3.6[##] 81–88 14.87%			20%
GIV	33.7 ±2.9[##] 30–37 61.32%			10%	39.0 ±2.9[##] 35–42 60.47%			10%
GV	13.3 ±1.8[##] 11–16 84.72%			0%	19.0±2.6[##] 15–23 80.74%			0%

F: F for one-way ANOVA test, pairwise comparison between each of the two groups was done using post hoc test (Tukey)
HS: highly significant (p<0.01)[##]: statistically significant at p ≤ 0.01 with infected control group (GII); R% = reduction percentage

Table 2. Serum levels of TAOC (pg/ml) during the murine intestinal and muscular phases of *T. spiralis* infection

Groups	Intestinal phase			Muscular phase		
	Mean ± SD range	F	P	Mean ± SD range	F	P
GI	0.4 ± 0.03 0.421–0.520	376.392	<0.001(HS)	0.4 ±0.02 0.461–0.531	421.649	<0.001(HS)
GII	0.2 ±0.1** 0.093–0.350			0.2 ±0.1** 0.097–0.321		
GIII	0.5 ±0.04## 0.520–0.610			0.5 ±0.03## 0.492–0.564		
GIV	1.2±0.06**## 1.19–1.33			1.2 ±0.06**## 1.197–1.326		
GV	1.7±0.1**## 1.640–1.88			1.7 ±0.09**## 1.620–1.802		

F: F for One way ANOVA test, pairwise comparison between each of the two groups was done using post hoc test (Tukey)
HS: highly significant (p<0.01)**: statistically significant at p ≤ 0.01 with healthy control group (GI)
##: statistically significant at p ≤ 0.01 with infected control group (GII)

The skeletal and lingual muscle findings

The skeletal and lingual muscles of GVb were infiltrated by a mild invasion of *Trichinella* larvae, which was accompanied by a mild inflammatory response of lymphocytes, macrophages, and eosinophils. Many of the larvae had entirely deteriorated and been replaced by inflammatory cells with normal muscle (Figure 3r, s), compared to GIIb, which had numerous encysted *Trichinella* larvae with a severe inflammatory hypersensitivity reaction and degenerative muscles surrounding it (Figure 3b, c). GIII showed severe invasion by encysted larvae surrounded by severe inflammatory reactions of eosinophils and round cells (Figure 3n, o). GIVb displayed moderate invasion by encysted *Trichinella* larvae surrounded by a moderate inflammatory reaction of eosinophils and round cells. Some larvae deteriorated and were replaced by inflammatory and transformed mesenchymal tissue (Figure 3p, q).

The ultrastructural changes of T. spiralis adults and larvae

SEM of adult *T. spiralis* revealed a severely collapsed body with a sloughed cuticle, loss of continuity, and normal arrangement of annulations with damaged copulatory bursa in GVa (Figure 4e, f) compared to the normal adult in GIIa (Figure 4a, b). The adults had a moderately collapsed body with a sloughed cuticle, loss of continuity, and normal arrangement of annulations with the appearance of carrions in GIIIa (Figure 4c), whereas a mild degree of collapse, loss of continuity, and regularity of transverse creases with multiple depressions and widening of bacillary openings was detected in GIV (Figure 4d). *T. spiralis* larvae in GVb had a severely damaged body and an entire sloughed cuticle with the appearance of multiple blebs and carrion. The larva was completely dead, with a complete loss of the normal annulations observed (Figure 4j) compared to the normal ones in GIIb (Figure 4g). GIVb showed a corrugated cuticle, moderate loss of transverse annulations of the posterior end, and the appearance of carrions at the cuticle (Figure 4i), while mild loss of cuticle striation was observed in GIIIb (Figure 4h).

Discussion

As the therapeutic efficacy of *Trichinella* infection drugs has yet to be satisfactorily shown (Sun *et al.* 2019), it is vital to develop novel, safe, and effective anti-*Trichinella* medicines. In this study, we evaluated the therapeutic efficacy of acetazolamide-loaded AgNPs on the intestinal and muscular phases of *T. spiralis* infection in mice.

For successful and early treatment of *Trichinella* infection, the eradication of intestinal forms represented by L1 larvae that within days develop into adults is substantial (Gottstein et al. 2009). Furthermore, commencing the treatment during the muscular phase is the most difficult since the drug must be in sufficient concentration within the muscles for subsequent absorption into the capsules. Given that passive diffusion is the primary method used to track drug absorption through the *T. spiralis* capsule, the effectiveness of a treatment against encysted larvae increases with drug concentration in the muscle. In this study, with respect to the reduction percentage in the number of adults and larvae, the groups treated with acetazolamide-loaded AgNPs provided the highest reduction percentages (84.72%–80.74%), respectively, compared to the untreated mice, followed by groups treated with acetazolamide with 61.32% and 60.47%, respectively, and then groups treated with nanoparticles (15.95%–14.87%). Acetazolamide efficacy was comparable to that observed by other researchers of *Trichinella* infection (Saad *et al.* 2016). An explanation for these findings could be that the CA inhibitor disrupted the usual detoxification of cyanate, elevating the intracellular cyanate content to lethal levels and causing the parasite to die (Zolfaghari-Emameh *et al.* 2015). Another explanation could be that inhibiting β-CA in parasite cells alters mitochondrial metabolic cycles, potentially eliminating pathogens (McKenna and Supuran 2014). Additionally, Zolfaghari-Emameh *et al.* (2014) hypothesised that inhibiting CA activity might delay cellular metabolic pathways within parasites.

The superiority of acetazolamide-loaded AgNPs can be explained by the special characteristics of nanoparticles that enhance drug absorption, increase drug bioavailability, increase cellular permeability, and decrease drug excretion from the body (Sun *et al.* 2019). Moreover, AgNPs had an antiparasitic impact as represented by the reduction in the ATP content of the cell, the damaging of mitochondria, and the increase in ROS production (Saini *et al.* 2016). Our findings agreed with Paredes *et al.* (2018), who noticed an improvement in the pharmacological characteristics of albendazole-loaded AgNPs, and with El-Melegy *et al.* (2019), who stated that AgNPs improve the therapeutic effect of
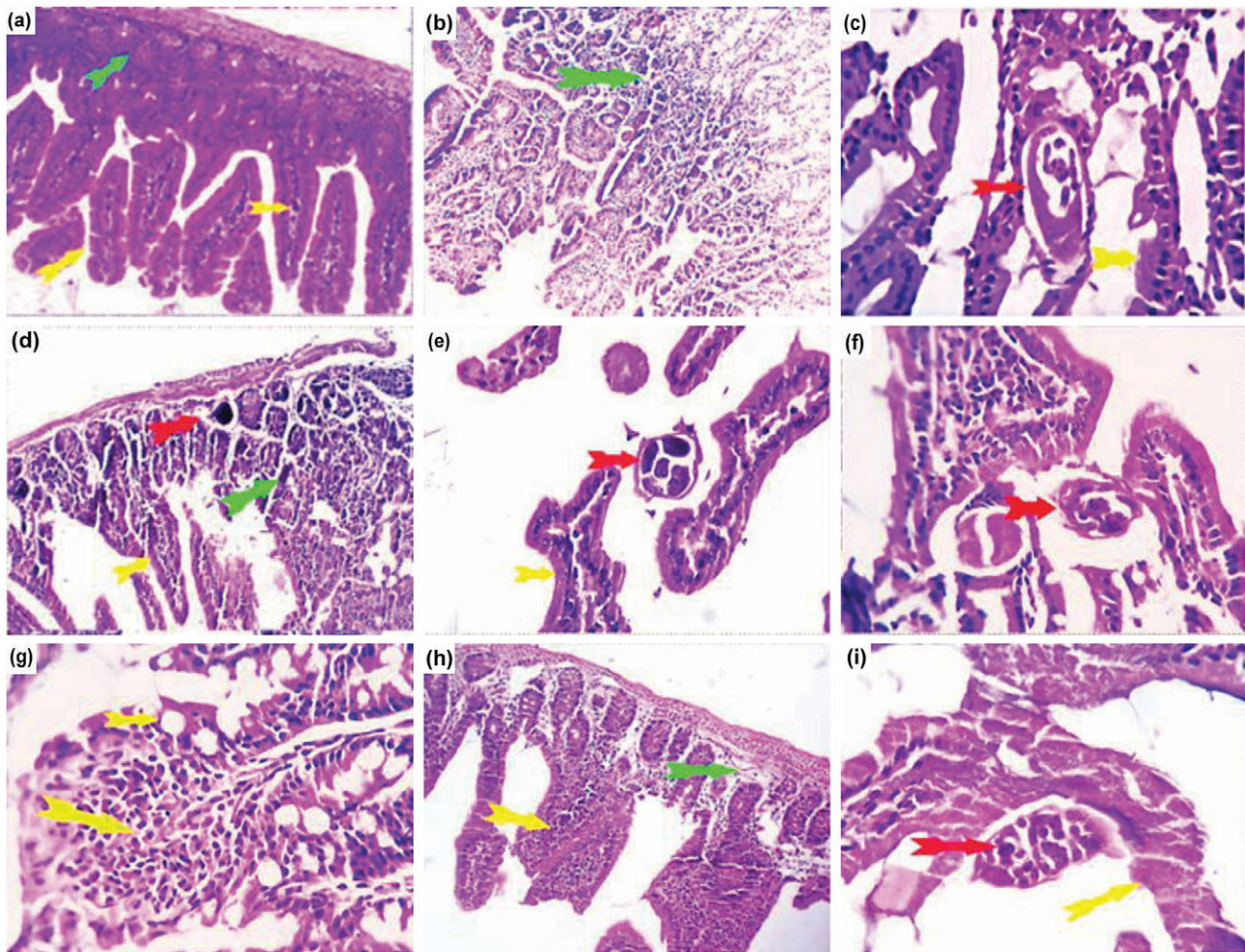
Figure 2. Histopathological results of *T. spiralis*-infected mice treated throughout the intestinal phase (H&E) (X 200& X 400). a: The small intestine of the normal control GIa showing normal histological structures of villi (yellow arrow), crypt, glands (green arrow), and mucosa and muscle layers. b, c: The small intestine of GIIa shows intense invasion by *T. spiralis* adults (red arrows); pressure atrophy in the cells is seen (yellow arrow). The surrounding intestinal mucosa showed mucosal edema and an excessive inflammatory reaction, mostly lymphocytes (green arrows). d, e: The small intestine of GIIIa shows invasion by *T. spiralis* adults (red arrows). The adjacent villous and mucosal epithelium suffered pressure atrophy (yellow arrows) with excessive mucosal and submucosal infiltration by lymphocytes and eosinophils (green arrows). f, g: The small intestine of GIVa shows moderate intramucosal invasion by *T. spirals* adults (red arrows). Moderate mucosal and submucosal infiltration by lymphocytes and eosinophils, goblet cells appear hyperreactive (yellow and green arrows). h, i: The small intestine of the targeted GVa shows mild mucosal invasion by degenerated *Trichinella* adults (red arrows). The intestinal villi are apparently normal in most parts (yellow arrows). Mild mucosal and submucosal infiltrations by lymphocytes, together with intact mucosa, were seen (green arrows).

mebendazole in *T. spiralis* infection. Likewise, AgNPs coated with anti-seizure drugs kill brain-eating amoebae, which are always fatal parasites (Anwar *et al.* 2019). Interestingly, acetazolamide-loaded AgNPs induced slightly higher percentage reductions in adults than in muscle larvae. This difference could be attributed to the timing of drug intake in relation to the affected *T. spiralis* stage. Besides, this effect may be due to some factors such as molting, changes in location, or basic biochemical differences in energy metabolism between the larval and adult stages (Yadav 2012).

Concerning the total antioxidant activity, the highest free-radical scavenging capacity in the sera of mice during the intestinal and muscular phases was observed in the targeted group given acetazolamide-loaded AgNPs, followed by the group given acetazolamide and AgNPs. These results highlighted the improvement in the host biochemical conditions in which *Trichinella* infection destroyed the antioxidant enzymatic systems and caused a disruption in metabolite homeostasis, as explained by a lower level of TAOC in the control infected group (Derda *et al.* 2003). These findings could be explained by AgNPs acting as catalysts with

antioxidant agents (Zhao *et al.* 2018), as they can exist in two oxidation states (Ag+ and Ag2+) depending on the reaction conditions, and the formed AgNPs may be able to quench free radicals by giving or absorbing electrons, acquiring silver nanoparticles antioxidant properties (Shanmugasundaram *et al.* 2013).

Pathological changes in the epithelium of the small intestine and skeletal muscles usually develop in trichinosis. Histopathological examination revealed that treatment with acetazolamide-loaded AgNPs ameliorated the *T. spiralis*-induced histopathological changes in the infected mice by reducing inflammatory cellular infiltration and restoring the normal villous structure. These findings were supported by Basyoni and El-Sabaa (2013), who suggested the higher effectiveness of different trichinicidal medications when given at an early stage. Our data also showed an improvement in the histopathological architecture of skeletal and lingual muscles in mice treated with acetazolamide-loaded AgNPs, including a decreased number of encysted larvae and their surrounding cellular infiltrates and increased regenerative muscles. Most larvae were degenerated and surrounded by mild
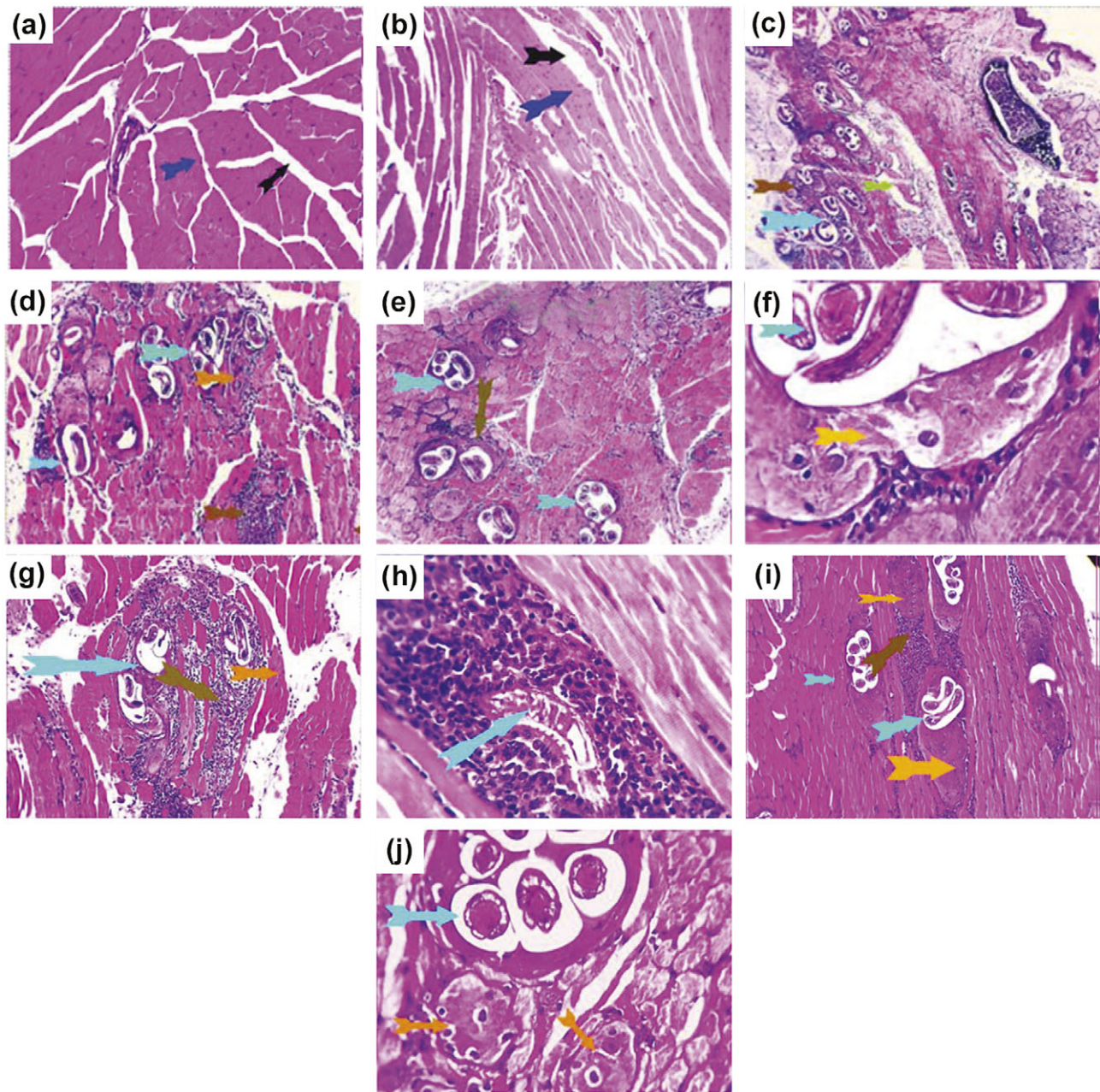
Figure 3. Histopathological results of *T. spiralis*-infected mice treated throughout the muscular phase (H, E) (X 200& X 400). j, k: muscles of normal control GIb showing normal histological structures with preserved longitudinal cross striations, peripherally situated multinuclear arrangement (blue arrows), interstitial tissue (black arrow), and tongue papillae. l, m: muscles GIIb show an invasion of encysted *Trichinella* larvae (light blue arrows). They were surrounded by an excessively inflammatory hypersensitivity reaction formed from eosinophils, lymphocytes, and macrophages (brown arrows). The surrounding muscle shows degenerative and necrotic changes besides the interstitial inflammatory edema (green). n, o: muscles of GIIIb showing severe invasion of the muscles by encysted larvae (light blue). They were surrounded by a severe inflammatory reaction of eosinophils and round cells (brown arrow) and transformed nuclei of the nurse cell (yellow arrow). The surrounding muscle denoted degenerative and necrotic changes, along with interstitial edema. p, q: muscles of GIVb showing moderate invasion by encysted *Trichinella* larvae (light blue arrow). They were surrounded by a moderate inflammatory reaction of lymphocytes, macrophages, and eosinophils (brown arrows). Some larvae were completely degenerated (q, blue arrows) and replaced by inflammatory cells. The surrounding muscle appears normal (orange arrow). r, s: muscles of the targeted GVb show mild invasion by encysted *Trichinella* larvae (light blue arrows). They were surrounded by a mild inflammatory reaction of eosinophils and round cells (brown arrows). Some of the larvae were degenerated and replaced by inflammatory and/or transformed mesenchymal tissue (fibrocartilagenous tissue) (orange arrows). The surrounding muscle showed mild degenerative changes (green arrow).

inflammatory reactions, reflecting the relative concentration of the drug in the muscle after administration of the formula. Acetazolamide-loaded AgNPs showed higher effectiveness compared to acetazolamide or AgNPs. This can be explained by the fact that AgNPs increase the therapeutic efficacy of acetazolamide drugs against *Trichinella* infection. AgNPs have unique physiochemical properties as anti-inflammatory (Panáček *et al.* 2009) and anti-angiogenesis (Rogers *et al.* 2008). Given that AgNPs have the ability to adhere to and be absorbed by the surface of targeted agents (Zayed *et al.* 2022), they can enter the intestinal intervillous spaces, providing a high local concentration of the drug on the surface of the membrane.
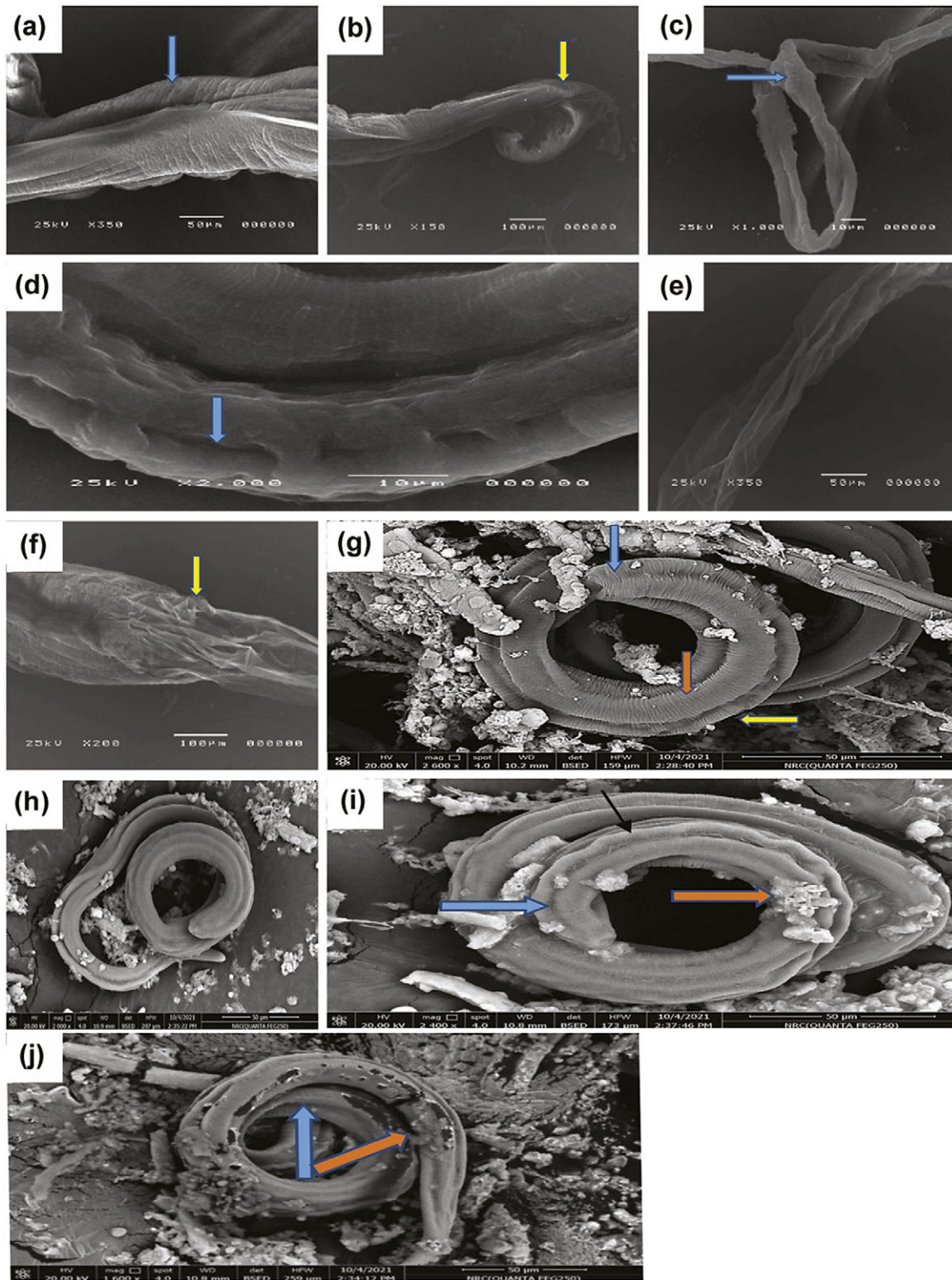
Figure 4. Scanning electron microscopy of *T. spiralis* adults and larvae.

a, b: Adults with GIIa show regular transverse creases with normal longitudinal ridges (blue arrow) and a normal copulatory bursa (yellow arrow). c: Adults of GIIIa show a moderately collapsed body with a sloughed cuticle, loss of continuity, and a normal arrangement of annulations with the appearance of carrion (blue arrow). d: Adults with GIVa have a mild degree of collapse and contraction without destruction. The cuticle also shows loss of continuity and regularity of transverse creases with multiple depressions and widening of bacillary openings (blue arrow). e, f: Adults of GVa show a severely collapsed body with a sloughed cuticle, loss of continuity, and normal arrangement of annulations with a damaged copulatory bursa (yellow arrow). g: GIIb showing the normal coiled appearance of the larva with normal annulations at the posterior end (blue arrow), normal transverse creases (brown arrow) along the body, and a normal longitudinal ridge with normal bacillary gland bands (yellow arrow). h: larva of GIIIb with mild loss of cuticle striation. i: larvae of GIVb show a corrugated cuticle (black arrows), moderate loss of transverse annulations of the posterior end (blue arrow), and the appearance of carrions at the cuticle (brown arrow). j: larva of GVb with severally damaged larvae and entirely sloughing of the cuticle, with the appearance of multiple blebs (blue arrows) and carrions (brown arrows). Additionally, a complete loss of the normal annulations was observed.

To confirm our results, *T. spiralis* adults and larvae of the targeted group given acetazolamide-loaded AgNPs were examined by SEM and proved to have severely damaged bodies, making them the most destroyed groups. Choi and Hu (2008) confirmed that nanoparticles disrupt the structure of glycoprotein and lipophosphoglycan molecules which are present on the surface of parasites and are responsible for the infection.

Conclusion

The results of our study showed that AgNPs are promising delivery systems for the oral administration of acetazolamide in the treatment of murine trichinellosis. Acetazolamide-loaded AgNPs had a lethal effect on adults and muscle larvae, generating significant in vivo damage, as proved histopathologically and ultrastructurally. None of the treatment strategies were able to completely eradicate the infection; however, acetazolamide-loaded AgNPs outperformed acetazolamide in the intestinal and muscle phases of *T. spiralis* infection.

References

Abou Rayia DM, Saad AE, Ashour DS, and Oreiby RM (2017) Implication of artemisinin nematicidal activity on experimental trichinellosis: in vitro and in vivo studies. *International Journal for Parasitology* **66**, 56–63. DOI: 10.1016/j.parint.2016.11.012

Akaike T, Suga M, and Maeda H (1998) Free radicals in viral pathogenesis: molecular mechanisms involving superoxide and NO. *Proceedings of the Society for Experimental Biology and Medicine* **217**, 64–73. DOI: 10.3181/00379727-217-44206

Allahverdiyev AM, Abamor ES, Bagirova M, Ustundag CB, Kaya C, Kaya F, and Rafailovich M (2011) Antileishmanial effect of silver nanoparticles and their enhanced antiparasitic activity under ultraviolet light. *International Journal of Nanomedicine* **6**, 2705. DOI: 10.2147/IJN.S23883

Anwar A, Rajendran K, Siddiqui R, Raza Shah M, and Mand Khan NA (2019) Clinically approved drugs against CNS diseases as potential therapeutic agents to target brain-eating amoebae. *ACS Chemical Neuroscience* **16**, 658–666. DOI: 10.1021/acschemneuro.8b00484

Bai X, Hu X, Liu X, Tang B, and Liu M (2017) Current research of trichinellosis in China. *Frontiers in Microbiology* **8**, 1472. DOI: 10.3389/fmicb.2017.01472

Basyoni MM and El-Sabaa AA (2013) Therapeutic potential of myrrh and ivermectin against experimental *Trichinella spiralis* infection in mice. *Korean Journal of Parasitology* **51**, 297–304. DOI: 10.3347/kjp.2013.51.3.297

Carleton MA, Drury GA, Willington EA, and Cammeron H (1967) *Carleton's histological technique.* 4th edn. New York, Toronto, London: Oxford Univ. Press. PMCID: PMC2385117.

Chen X, Yang Y, Yang J, Zhang Z, and Zhu X (2012) RNAi-mediated silencing of paramyosin expression in *Trichinella spiralis* results in impaired viability of the parasite. *PLoS One* **7**, e49913. https://doi.org/10.1371/journal.pone.0049913

Choi O and Hu Z (2008) Size dependent and reactive oxygen species related nanosilver toxicity to nitrifying bacteria. *Environmental Science & Technology* **42**, 4583–4588. https://doi.org/10.1021/es703238h

Collins AR (2005) Assays for oxidative stress and antioxidant status: applications to research into the biological effectiveness of polyphenols. *The American Journal of Clinical Nutrition* **81**(Suppl **1**), 261–267. DOI: 10.1093/ajcn/81.1.261S

Denham DA (1965) Studies with methyridine and *Trichinella spiralis.* I. Effect upon the intestinal phase in mice. *Experimental Parasitology* **17**, 1014. DOI: 10.1016/0014-4894(65)90003-2

Derda M, Boczoń K, Wandurska-Nowak E, and Wojt W (2003) Changes in the activity of glutathione-S-transferase in muscles and sera from mice infected with *Trichinella spiralis* after treatment with albendazole and levamisole. *Parasitology Research* **89**, 509–512. DOI: 10.1007/s00436-002-0825-y

Dupouy-Camet J (2014) Travels and tourism are drivers for trichinellosis. *Parasitologists United Journal* **7**, 86–92. http://www.new.puj.eg.net/text.asp?2014/7/2/86/149555

Eid RK, Ashour DS, Essa EA, El Maghraby GM, and Arafa MF (2020) Chitosan coated nanostructured lipid carriers for enhanced in vivo efficacy of albendazole against *Trichinella spiralis. Carbohydrate Polymers* **232**, 115826. DOI: 10.1016/j.carbpol.2019.115826

Eissa MM, El-Azzouni MZ, Mady RF, Fathy FM, and Baddour NM (2012) Initial characterization of an autoclaved *Toxoplasma* vaccine in mice. *Experimental Parasitology* **131**, 310–316. DOI: 10.1016/j.exppara.2012.05.001

Elmelegy MA, Ghoneim NS, El Dien N, and Rizk MS (2019) Silver nano particles improve the therapeutic effect of mebendazole treatment during the muscular phase of experimental trichinellosis. *The Journal of American Science* **15**, 34-. DOI: 10.7537/marsjas150519.06

Elmi T, Gholami S, Fakhar M, and Azizi F (2013) A review on the use of nanoparticles in the treatment. *Journal of Mazandaran University of Medical Science* **23**, 126–133. URL: http://jmums.mazums.ac.ir/article-1-2396-en.html

Fisker R, Carstensen JM, Hansen MF, Bødker F, and Mørup S (2000) Estimation of nanoparticle size distributions by image analysis. *Journal of Nanoparticle Research* **2**, 267–277. DOI:10.1023/A:1010023316775

Gherbawy YA, Shalaby IM, Abd El-Sadek MS, Elhariry HM, and Banaja AA (2013) The anti-fasciolasis properties of silver nanoparticles produced by *Trichoderma harzianum* and their improvement of the anti-fasciolasis drug triclabendazole. *International Journal of Molecular Sciences* **14**, 21887–21898. DOI: 10.3390/ijms141121887

Ghiselli A, Serafini M, Natella F, and Scaccini C (2000) Total antioxidant capacity as a tool to assess redox status: critical view and experimental data. *Free Radical Biology and Medicine* **29**, 1106–1114. DOI: 10.1016/s0891-5849(00)00394-4

Gottstein B, Pozio E, and Nockler K (2009) Epidemiology, diagnosis, treatment, and control of trichinellosis. *Clinical Microbiology Reviews* **22**(**1**),127–45. DOI: 10.1128/CMR.00026-08

Issa RM, El-Arousy MH, and Abd EI-Aal AA (1998) Albendazole: a study of its effect on experimental *Trichinella spiralis* infection in rats. *Egyptian Journal of Medical Sciences* **19**, 281–290.

Luis Muñoz-Carrillo J, Maldonado-Tapia C, López-Luna A, Jesús Muñoz Escobedo J, Armando Flores-De La Torre J, Moreno-García A (2019) Current aspects in Trichinellosis. p. 175–216 in *Parasites and Parasitic Diseases.* London, UK, IntechOpen.

Mckenna R and Supuran CT (2014) Carbonic anhydrase inhibitors drug design. *Sub-Cellular Biochemistry* **75**, 291–323. DOI: 10.1007/978-94-007-7359-2_15

Mulfinger L, Solomon SD, Bahadory M, Jeyarajasingam AV, Rutkowsky SA, and Boritz C (2007) Synthesis and study of silver nanoparticles. *Journal of Chemical Education* **84**, 322. DOI: https://doi.org/10.1021/ed084p322

Mulvaney P (1996) Surface plasmon spectroscopy of nanosized metal particles. *Langmui* **12**, 788–800. DOI: https://doi.org/10.1021/la9502711

Panáček A, Kolář M, Večeřová R, Prucek R, Soukupová J, Kryštof V, Hamal P, Zbořil R, and Kvítek L (2009) Antifungal activity of silver nanoparticles against Candida spp. *Biomaterials* **30**, 6333–6340. DOI: 10.1016/j.biomaterials07.065

Paredes AJ, Litterio N, Dib A, Allemandi DA, Lanusse C, Bruni SS, and Palma SD (2018) A nanocrystal-based formulation improves the pharmacokinetic performance and therapeutic response of albendazole in dogs. *Journal of Pharmacy and Pharmacology* **70**, 51–58. DOI: 10.1111/jphp.12834

Rogers JV, Parkinson CV, Choi YW, Speshock JL, and Hussain SM (2008) A preliminary assessment of silver nanoparticle inhibition of monkeypox virus plaque formation. *Nanoscale Research Letters* **3**, 129–133. DOI: 10.1007/s11671-008-9128-2

Pozio E (2015) *Trichinella* spp. imported with live animals and meat. *Veterinary Parasitology* **213**, 46–55. DOI: 10.1016/j.vetpar.2015.02.017

Saad AE, Ashour DS, Abou Rayia DM, and Bedeer AE (2016) Carbonic anhydrase enzyme as a potential therapeutic target for experimental trichinellosis. *Parasitology Research* **115**, 2331–2339. DOI: 10.1007/s00436-016-4982-9

Saad AHA, Soliman MI, Azzam AM, and Mostafa AB (2015) Antiparasitic activity of silver and copper oxide nanoparticles against *Entamoeba histolytica* and *Cryptosporidium parvum* cysts. *Journal of the Egyptian Society of Parasitology* **45**, 593–602. DOI: 10.12816/0017920

Saini P, Saha SK, Roy P, Chowdhury P, and Babu SPS (2016) Evidence of reactive oxygen species (ROS) mediated apoptosis in Setaria cervi induced by green silver nanoparticles from Acacia auriculiformis at a very low dose. *Experimental Parasitology* **160**, 39–48. DOI: 10.1016/j.exppara.2015.11.004

Shanmugasundaram T, Radhakrishnan M, Gopikrishnan V, Pazhanimurugan R, and Balagurunathan R (2013) A study of the bactericidal, anti-biofouling, cytotoxic and antioxidant properties of actinobacterially synthesised silver nanoparticles. *Colloids and Surfaces B: Biointerfaces* **111**, 680–687. DOI: 10.1016/j.colsurfb.2013.06.045

Sun Y, Chen D, Pan Y, Qu W, Hao H, Wang X, Liu Z, and Xie S (2019) Nanoparticles for antiparasitic drug delivery. *Drug Delivery* **26**, 1206–1221. DOI: 10.1080/10717544.2019.1692968

Syrjänen L, Tolvanen M, Hilvo M, Olatubosun A, Innocenti A, Scozzafava A, Leppiniemi J, Niederhauser B, Hytönen VP, and Gorr TA (2010) Characterization of the first beta-class carbonic anhydrase from an arthropod (*Drosophila melanogaster*) and phylogenetic analysis of beta-class carbonic anhydrases in invertebrates. *BMC Biochemistry* **11**, 1–13. DOI: 10.1186/1471-2091-11-28

Wang M, Chen J, Liu C, Qiu J, Wang X, Chen P, and Xu C (2017) A graphene quantum dots–hypochlorite hybrid system for the quantitative fluorescent determination of total antioxidant capacity. *Small* **13**, 1700709. DOI: 10.1002/smll.201700709

Yadav AK and Temjenmongla (2012) Efficacy of Lasia spinosa leaf extract in treating mice infected with *Trichinella spiralis*. *Parasitology Research* **110**, 493–498. DOI: 10.1007/s00436-011-2551-9

Younis MS, Abououf EER, Ali AES, Abd elhady SM, and Wassef RM (2020) in vitro effect of silver nanoparticles on *Blastocystis hominis*. *International Journal of Nanomedicine* 8167–8173. DOI: 10.2147/IJN.S272532

Zayed KM, Guo YH, Lv S, Zhang Y, and Zhou XN (2022) Molluscicidal and antioxidant activities of silver nanoparticles on the multi-species of snail intermediate hosts of schistosomiasis. *PLOS Neglected Tropical Diseases* **16**, e0010667. DOI: 10.1371/journal.pntd.0010667

Zhao X, Zhou L, Riaz Rajoka MS, Yan L, Jiang C, Shao D, Zhu J, Shi J, Huang Q, and Yang H (2018) Fungal silver nanoparticles: synthesis, application and challenges. *Critical Reviews in Biotechnology* **38**, 817–835. DOI: 10.1080/07388551.2017.1414141

Ziel R, Haus A, and Tulke A (2008) Quantification of the pore size distribution (porosity profiles) in microfiltration membranes by SEM, TEM and computer image analysis. *Journal of Membrane Science* **323**, 241–246. DOI: https://doi.org/10.1016/j.memsci.2008.05.057

Emameh RZ, Barker H, Hytönen VP, Tolvanen ME, and Parkkila S (2014) Beta carbonic anhydrases: novel targets for pesticides and anti-parasitic agents in agriculture and livestock husbandry. *Parasites & Vectors* **7**, 1–11. DOI: 10.1186/1756-3305-7-403

Emameh RZ, Kuuslahti M, Vullo D, Barker HR, Supuran CT, and Parkkila S (2015) *Ascaris lumbricoides* β carbonic anhydrase: a potential target enzyme for treatment of ascariasis. *Parasites & Vectors* **8**, 1–10. DOI: 10.1186/s13071-015-1098-5